Electronic Supplementary Material (ESI) for Dalton Transactions.

Supporting Information

Towards highly active and stable Nickel-based Metal-Organic Frameworks as Ethylene Oligomerization Catalysts

Ubed SF. Arrozi[a], Volodymyr Bon[a], Christel Kutzscher[a], Irena Senkovska[a], Stefan Kaskel[a]

Technische Universität Dresden, Department of Chemistry, Institute of Inorganic Chemistry, Bergstraße 66, D-01062 Dresden, Germany

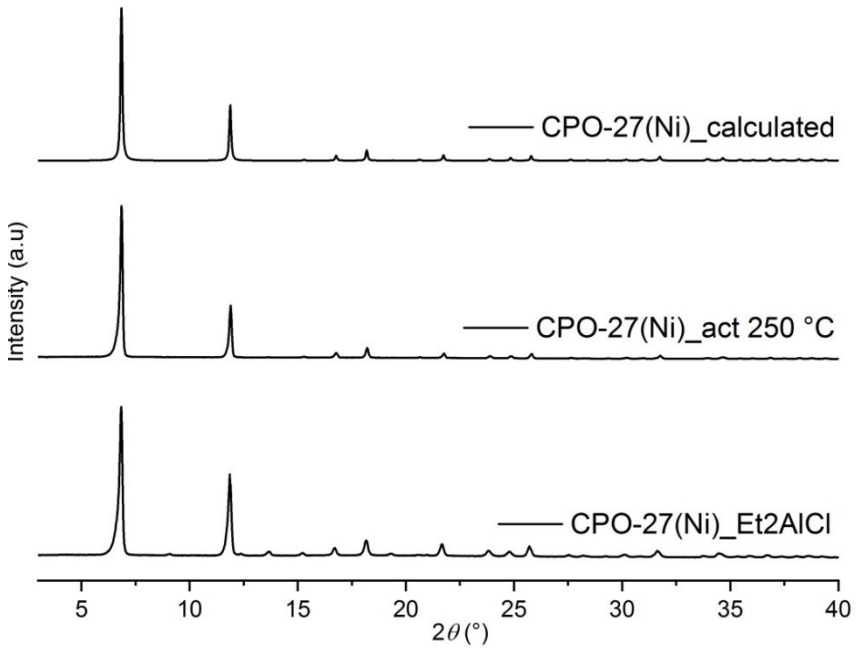

Figure S1. PXRD patterns of CPO-27(Ni) (**1**): theoretical pattern calculated from the crystal structure, [CCDC 288477] (top); after desolvation at 250 °C in vacuum (middle), after stirring in toluene in the presence of the Et_2AlCl overnight (bottom).

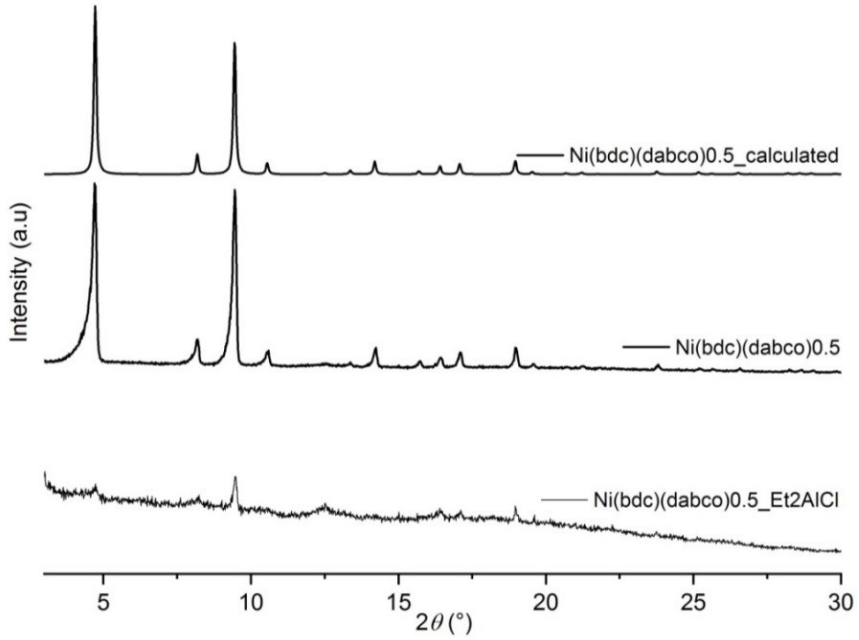

Figure S2. PXRD patterns of $[Ni(bdc)(dabco)_{0.5}]_n$ **(4)**: theoretical pattern calculated from the crystal structure, CCDC 802893 (top); activated $[Ni(bdc)(dabco)_{0.5}]_n$ (middle), after stirring in toluene in the presence of the Et_2AlCl overnight (bottom).

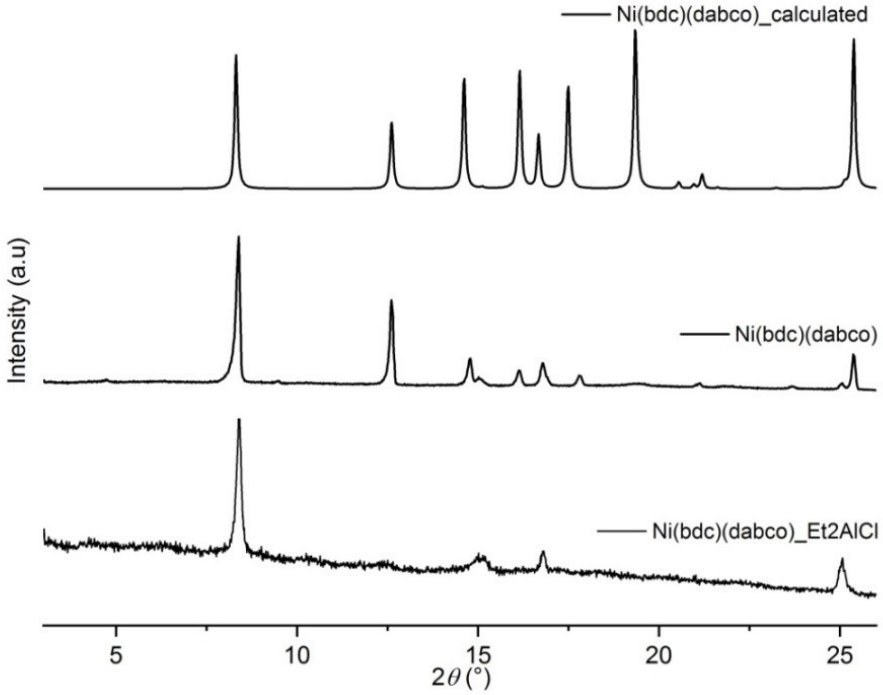

Figure S3. PXRD patterns of $[Ni(bdc)(dabco)]_n$ (**2**): theoretical pattern calculated from the crystal structure (top) [CCDC 802894]; activated (middle), after stirring in toluene in the presence of the Et_2AlCl overnight (bottom).

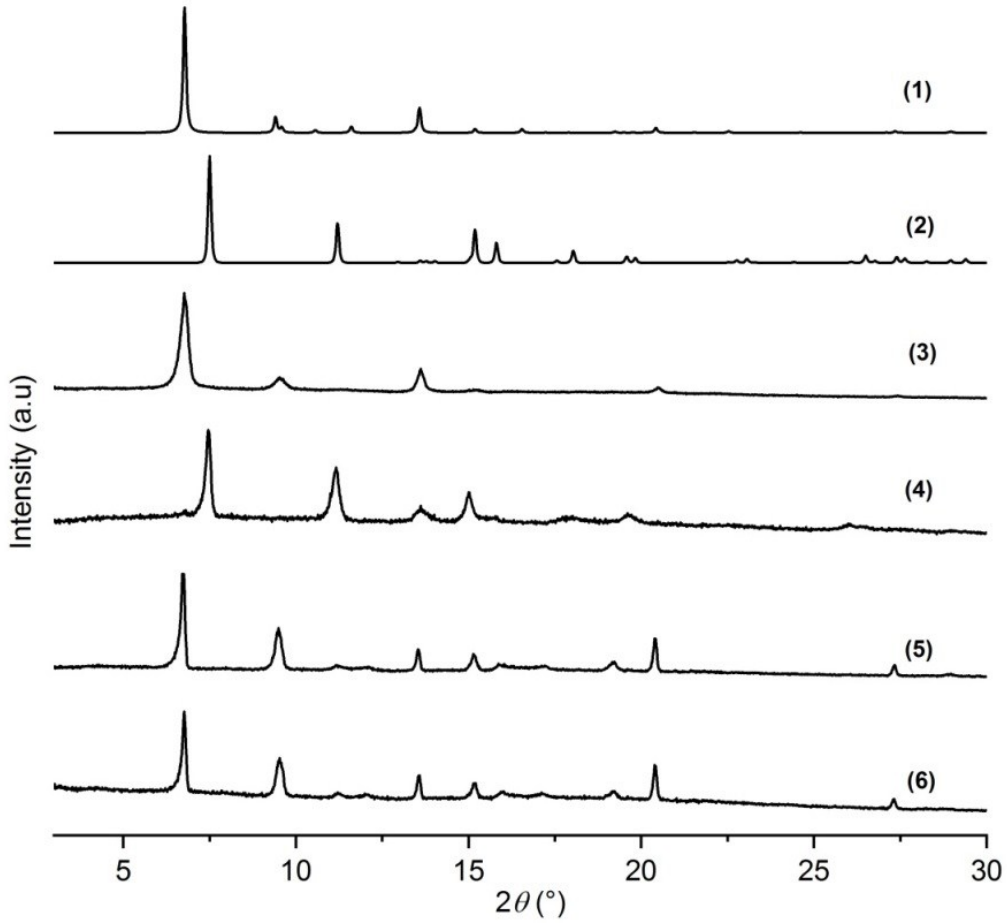

Figure S4. PXRD patterns of $[Ni(ndc)(dabco)_{0.5}]_n$ (DUT-8(Ni)) (**5/6**): theoretical pattern of the open pore form of DUT-8(Ni) calculated from the crystal structure [CCDC 760964] (1); theoretical pattern of the closed pore form DUT-8(Ni) calculated from the crystal structure [CCDC 1034317] (2); activated DUT-8(Ni)_rigid (3); activated DUT-8(Ni)_flexible (4); DUT-8(Ni)_flexible compound stirred in toluene (showing the opening of the pores) (5); and DUT-8(Ni)_rigid after stirring in toluene in the presence of the Et_2AlCl overnight (6).

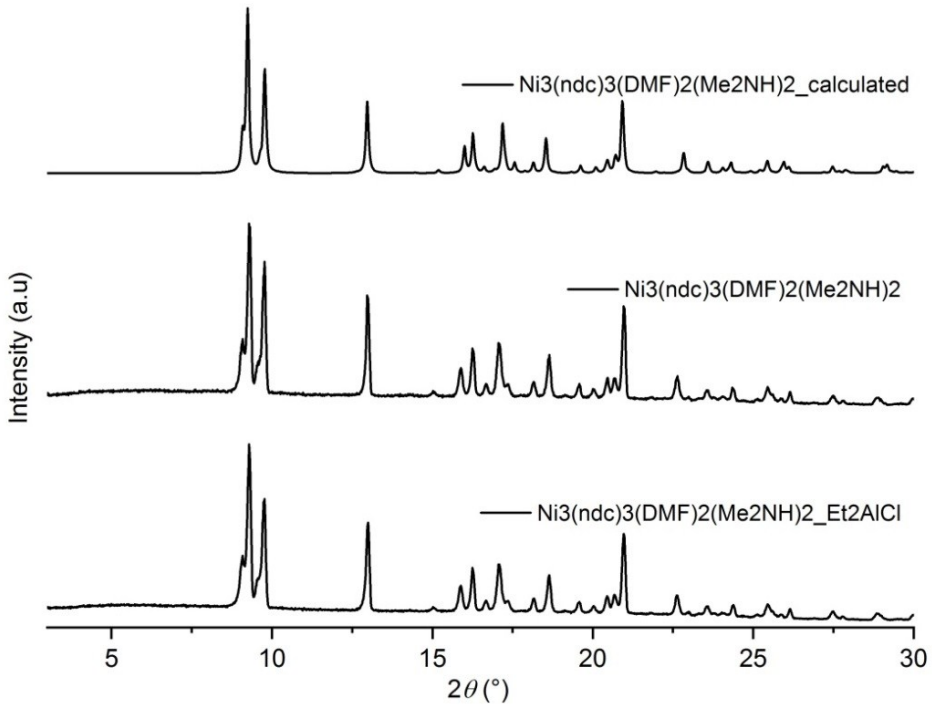

Figure S5. PXRD patterns of $[Ni_3(ndc)_3(DMF)_2((CH_3)_2NH)_2]_n$ (**3**): theoretical pattern calculated from the crystal structure [CCDC 759306] (top); activated (middle), after stirring in toluene in the presence of the Et_2AlCl overnight (bottom).

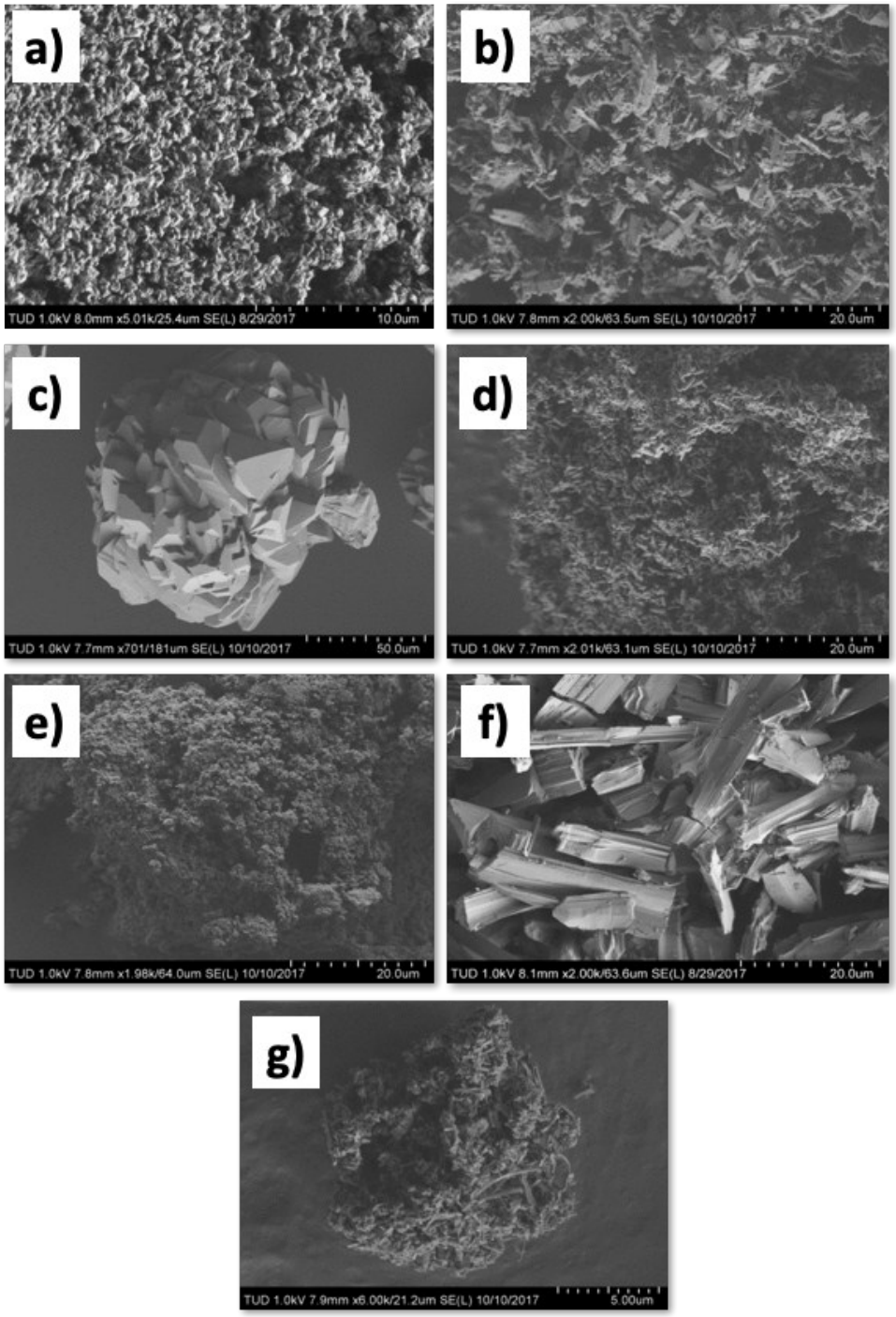

Figure S6. SEM images of: a) CPO-27(Ni) **(1)**, b) $[Ni(bdc)(dabco)]_n$ (**2**), c) $[Ni_3(ndc)_3(DMF)_2((CH_3)_2NH)_2]_n$ (**3**), d) $[Ni(bdc)(dabco)_{0.5}]_n$ (**4**); e) DUT-8(Ni)_rigid (**5**), f) DUT-8(Ni)_flexible (**6**), and g) DUT-128 **(7)**. ImageJ software package was used to calculate crystal size distribution.

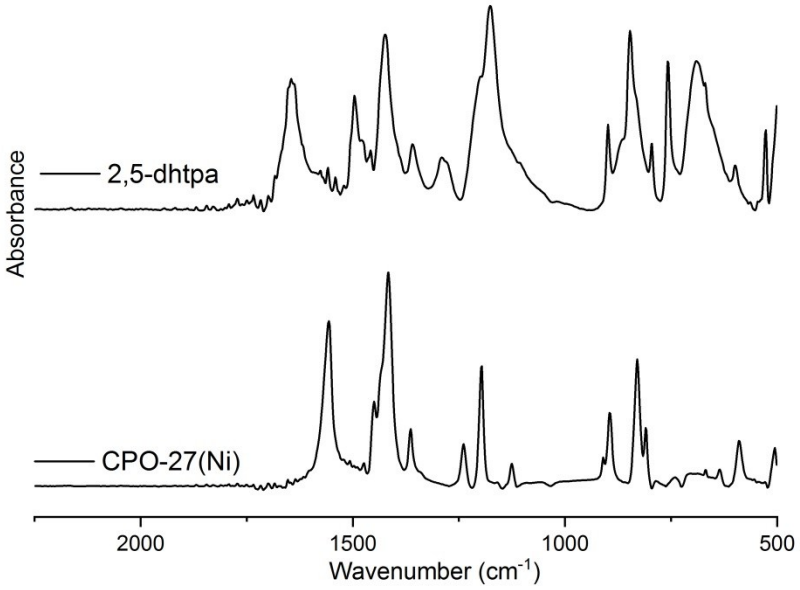

Figure S7. ATR-IR spectra of 2,5-dihydroxyterephthalic acid (2,5-dhtpa) (top) and CPO-27(Ni) **(1)** (bottom).

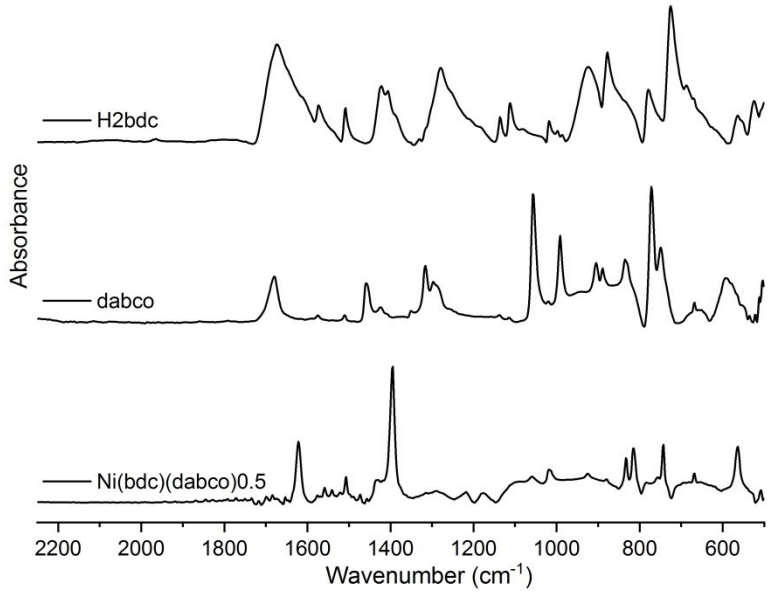

Figure S8. ATR-IR spectra of 1,4-benzenedicarboxylic acid (H_2bdc) (top) and $[Ni(bdc)(dabco)_{0.5}]_n$ **(4)** (bottom).

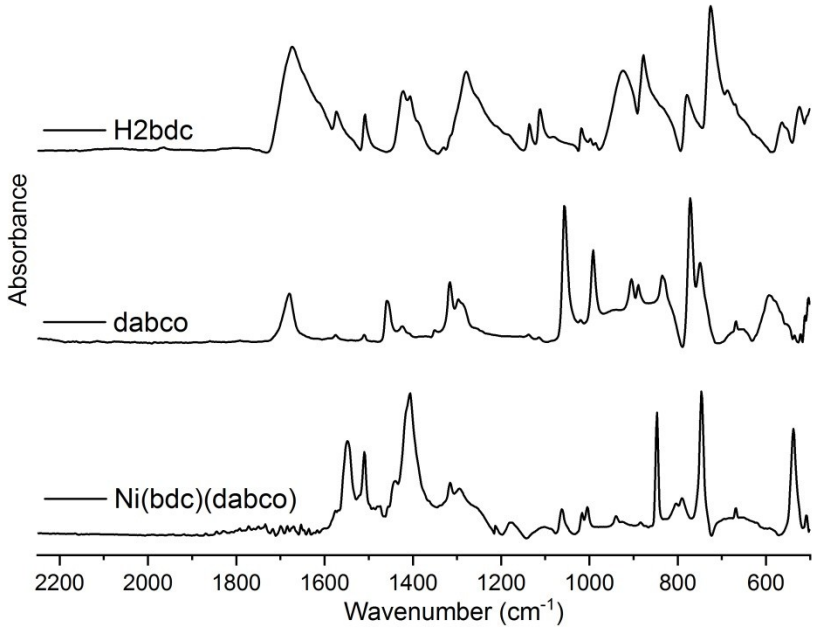

Figure S9. ATR spectra of 1,4-benzenedicarboxylic acid (H_2bdc) (top), dabco (middle) and $[Ni(bdc)(dabco)]_n$ **(2)** (bottom).

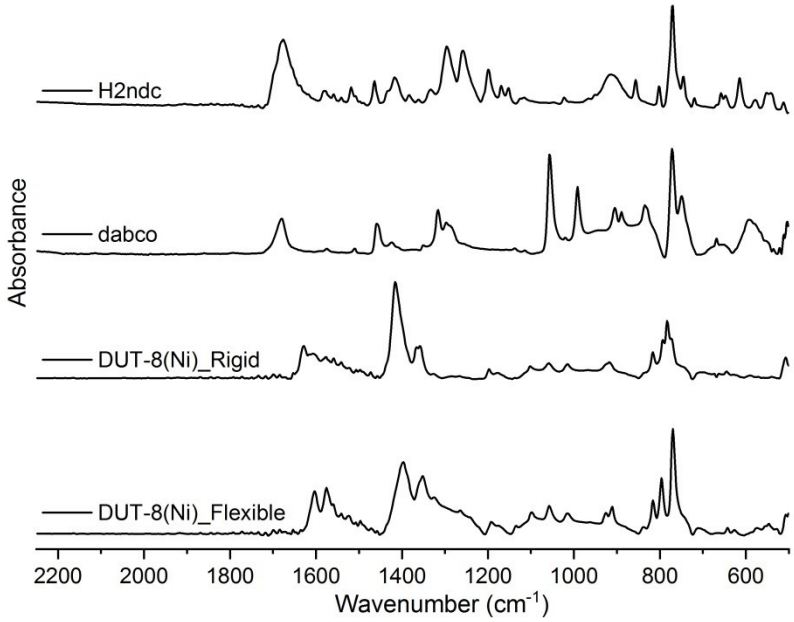

Figure S10. ATR-IR spectra (from top to bottom) of 2,6-naphtalenedicarboxylic acid (H_2ndc), dabco, $[Ni(ndc)(dabco)_{0.5}]_n$_rigid (DUT-8(Ni)_rigid, **5**) and $[Ni(ndc)(dabco)_{0.5}]_n$_flexible (DUT-8(Ni)_flexible, **6**).

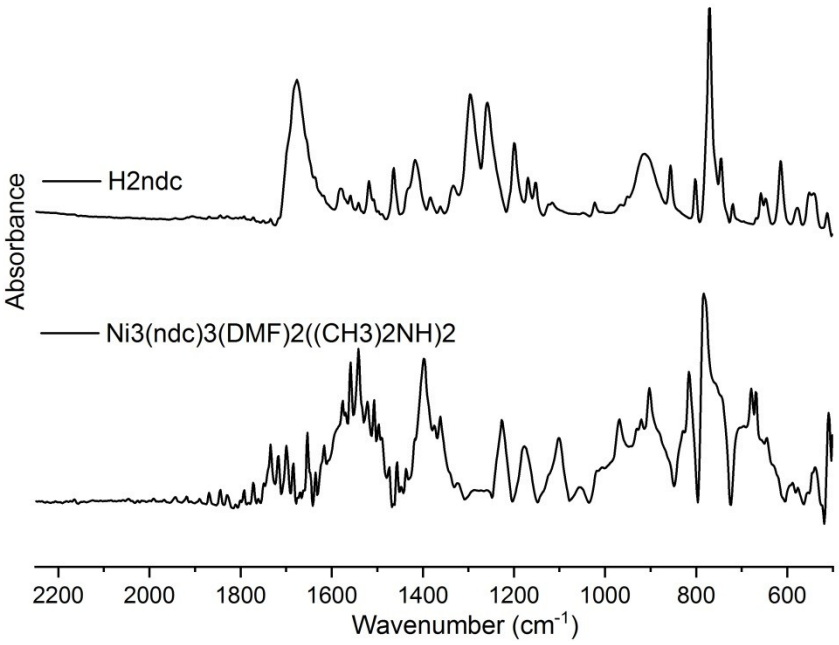

Figure S11. ATR spectra of 2,6-naphtalenedicarboxylic acid (H_2ndc) (top) and $[Ni_3(ndc)_3(DMF)_2((CH_3)_2NH)_2]_n$ (**3**) (bottom).

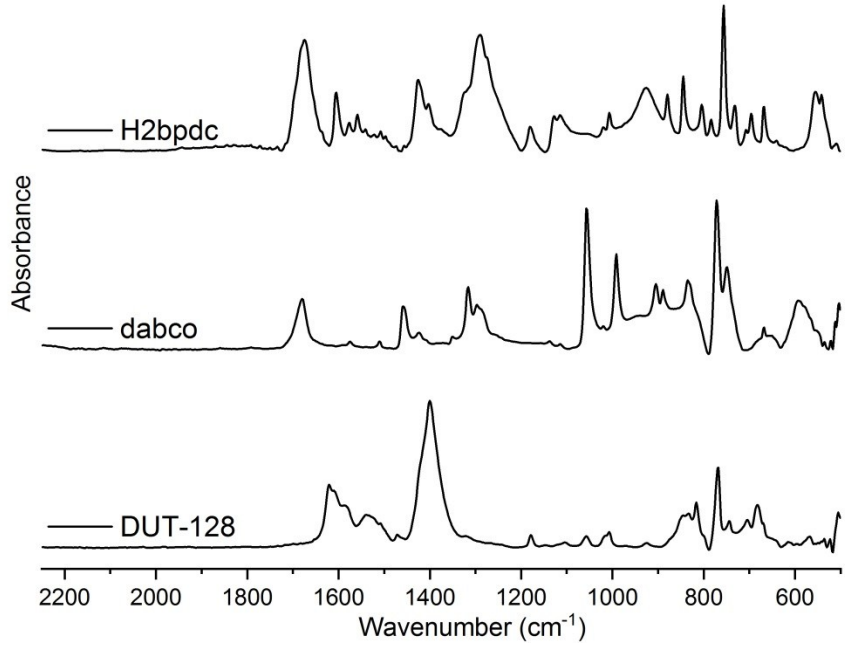

Figure S12. ATR spectra of 4,4′-biphenyldicarboxylic acid (H_2bpdc) (top), dabco (middle) and DUT-128 (**7**) (bottom).

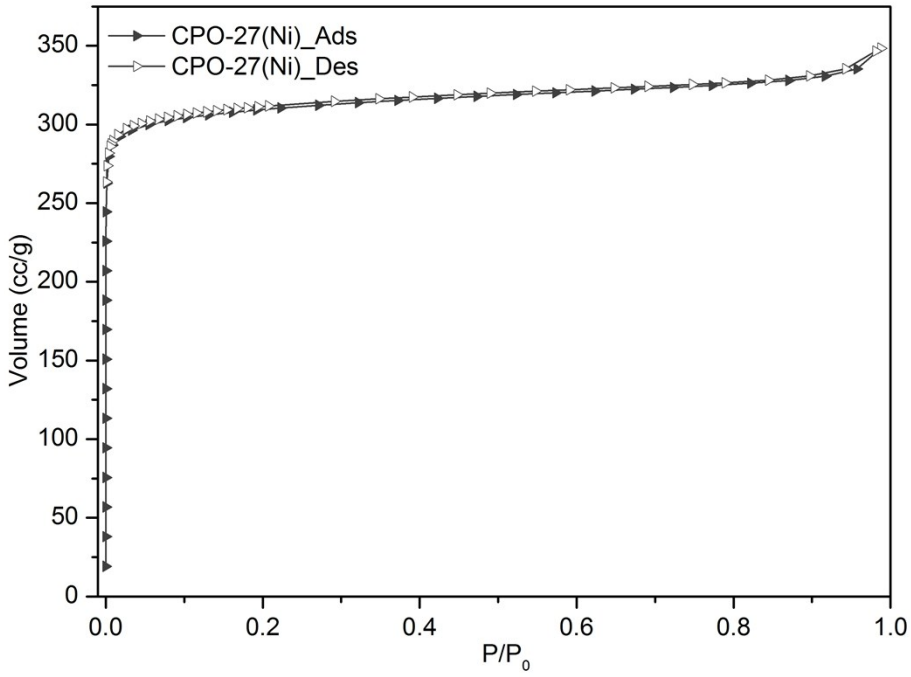

Figure S13. N_2 physisorption isotherm of CPO-27(Ni) (**1**) at 77 K. Solid symbols – adsorption, empty symbols – desorption.

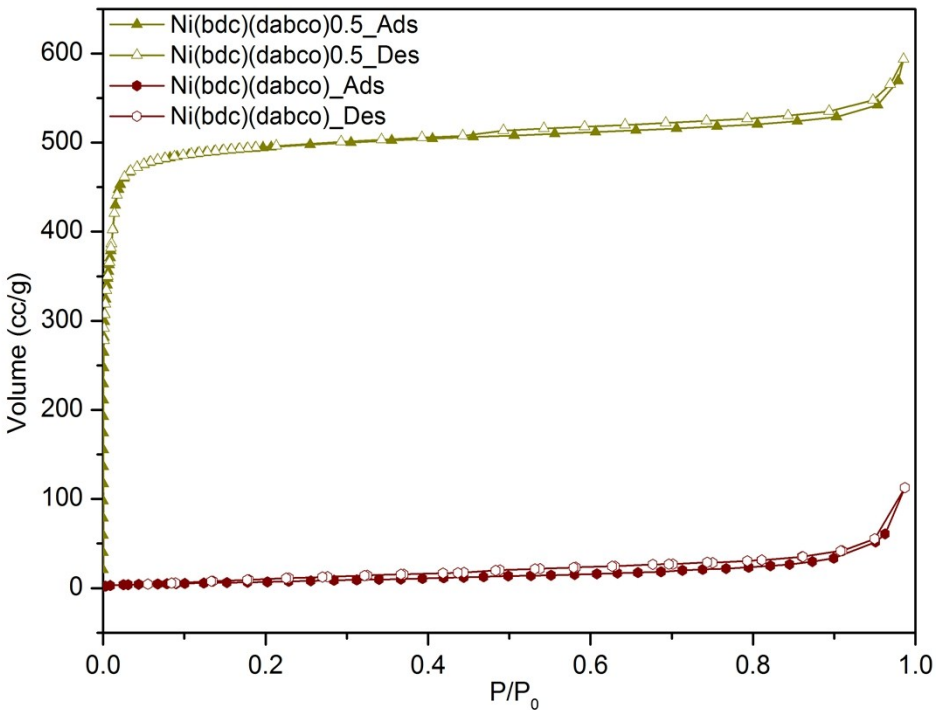

Figure S14. N_2 physisorption isotherms of $[Ni(bdc)(dabco)]_n$ (**2**) and $[Ni(bdc)(dabco)_{0.5}]_n$ (**4**) at 77 K. Solid symbols – adsorption, empty symbols – desorption.

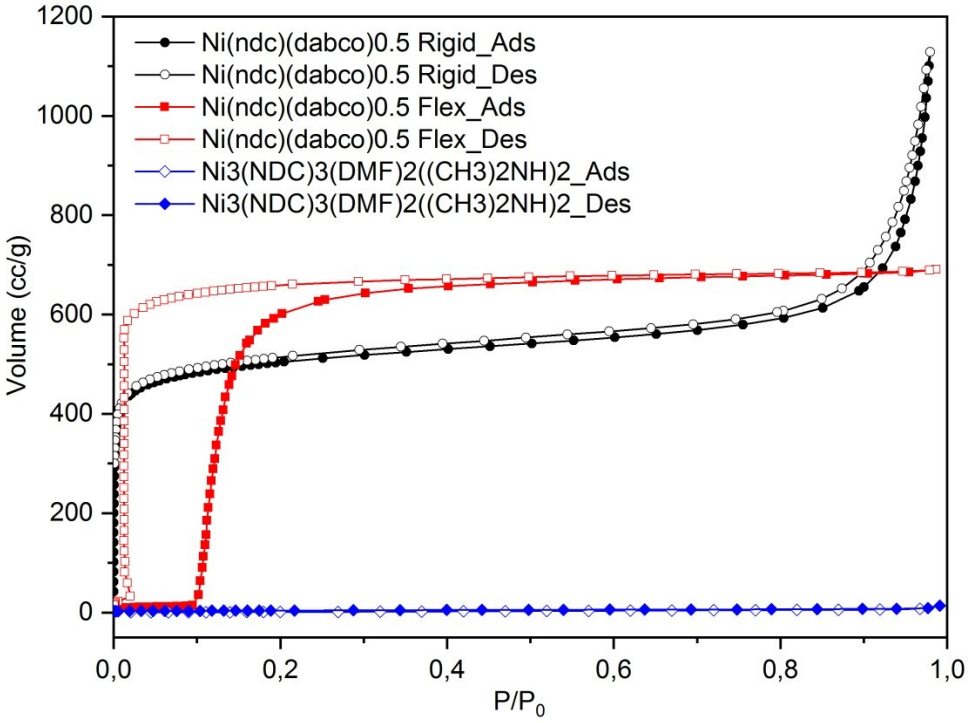

Figure S15. N_2 physisorption isotherms of $[Ni_3(ndc)_3(DMF)_2((CH_3)_2NH)_2]_n$ (**3**) (blue), DUT-8(Ni)_rigid (**5**) (black), DUT-8(Ni)_flexible (**6**) (red), and at 77 K. Solid symbols – adsorption, empty symbols – desorption.

Table S1. Surface area and pore volume of investigated Ni-MOFs.

Ni-MOFs	BET area (m^2g^{-1})	Pore volume (cm^3g^{-1})
CPO-27(Ni) (**1**)	1223	0.5
$[Ni(bdc)(dabco)]_n$ (**2**)	19	0.1
$[Ni_3(ndc)_3(DMF)_2((CH_3)_2NH)_2]_n$ (**3**)	12	0.02
$[Ni(bdc)(dabco)_{0.5}]_n$ (**4**)	1983	0.9
DUT-8(Ni)_rigid (**5**)	1899	0.9
DUT-8(Ni)_flexible (**6**)	-	1.0
DUT-128 (**7**)	850	0.8

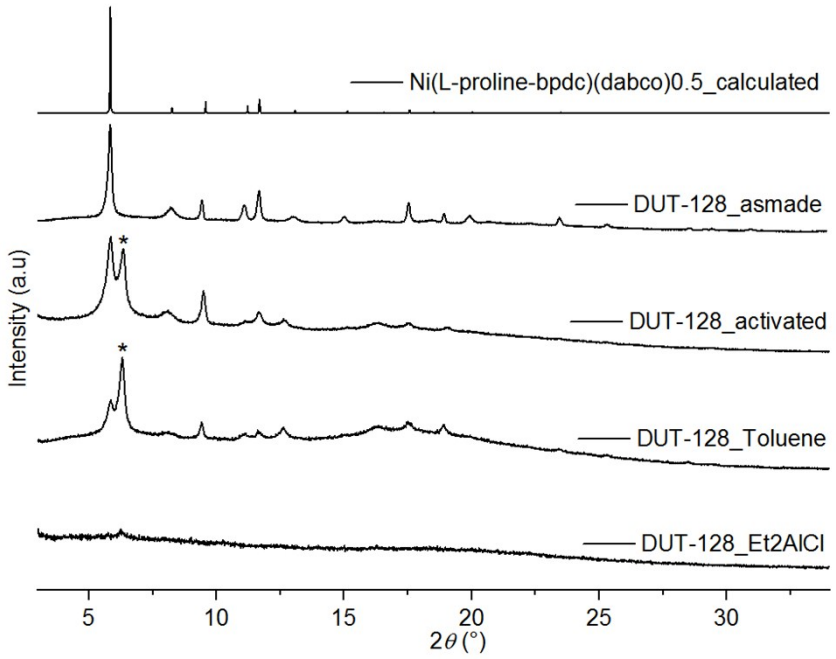

Figure S16. PXRD patterns of DUT-128 **(7)** from top to bottom: theoretical PXRD pattern of $[Ni(L\text{-proline-bpdc})(dabco)_{0.5}]_n$ [CCDC 1835717]; DUT-128 as-made; DUT-128 activated; activated DUT-128 immersed in toluene; and DUT-128 after stirring in toluene in the presence of the Et_2AlCl overnight. The new peak (*) in the PXRD patterns of activated sample and sample after immersion in toluene can be assigned to the closed pore phase as observed for DUT-8(Ni).

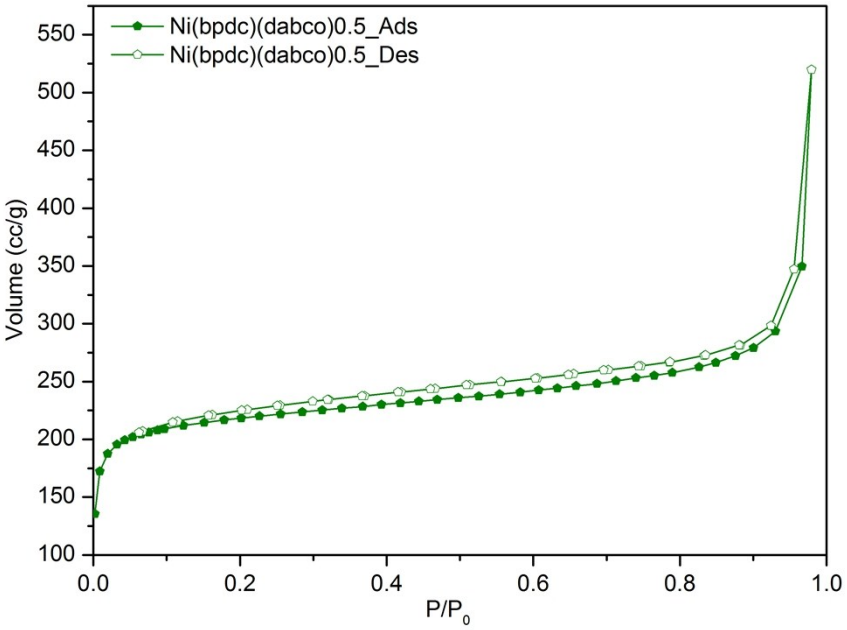

Figure S17. N_2 physisorption isotherm of DUT-128 **(7)** at 77 K. Solid symbols – adsorption, empty symbols – desorption.

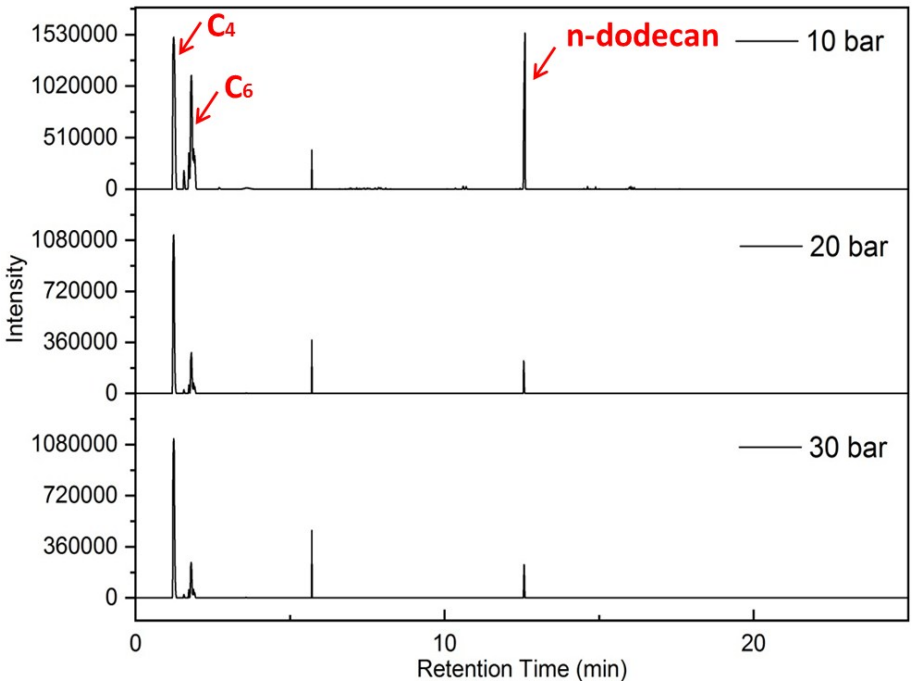

Figure S18. Typical chromatogram of products formed in ethylene oligomerization reaction catalyzed by DUT-8(Ni)_rigid **(5)** at 10 bar (top), 20 bar (middle), and 30 bar (bottom).

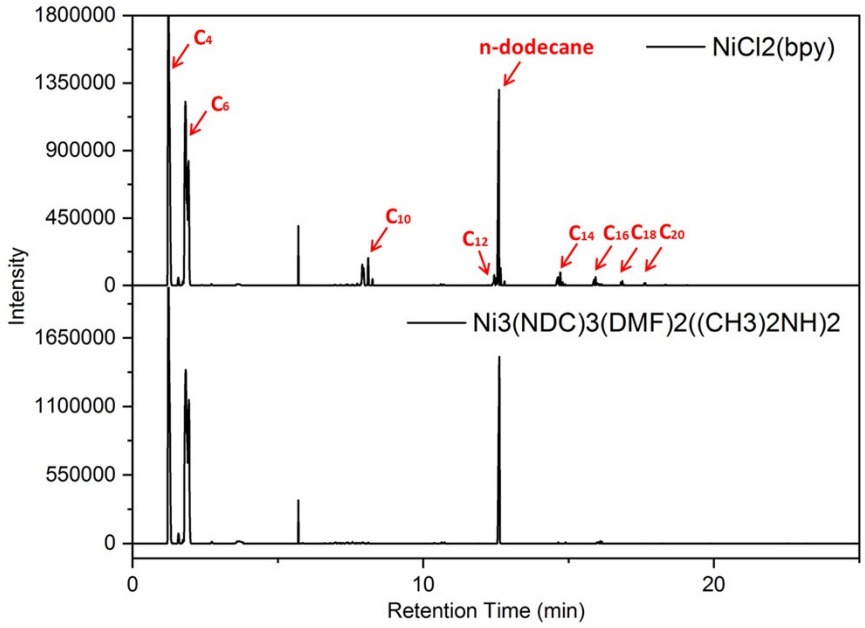

Figure S19. Typical chromatogram of the cyclic reaction products catalyzed by [$NiCl_2$(bpy)] (top) and [$Ni_3(ndc)_3(DMF)_2((CH_3)_2NH)_2]_n$ (**3**) (bottom). C_8 oligomers could not be detected due to the peak overlap with broad signal of the toluene.

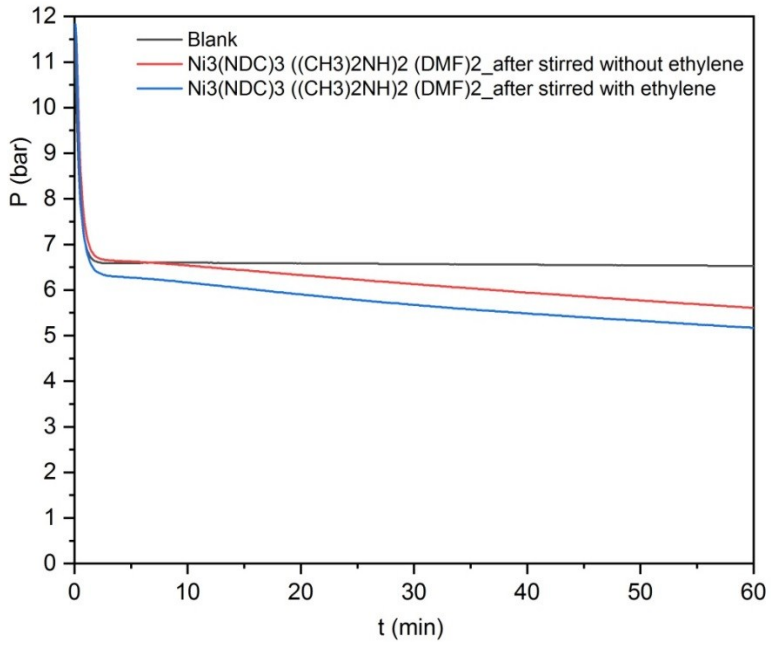

Figure S20. Ethylene consumption in leaching test using $[Ni_3(ndc)_3(DMF)_2((CH_3)_2NH)_2]_n$ (**3**) as catalyst.

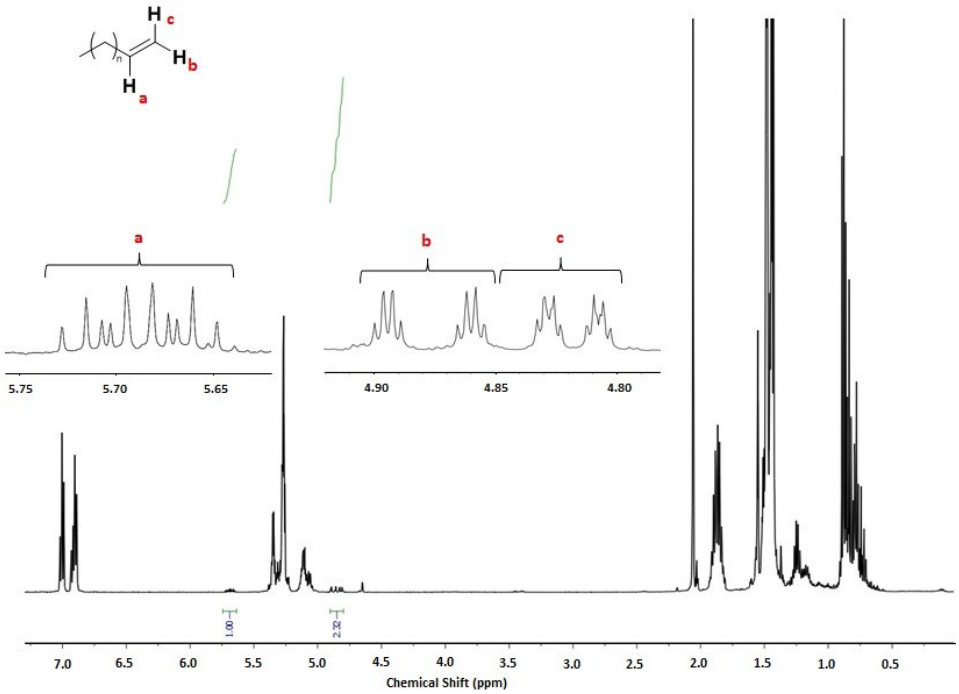

Figure S21. ^{1}H NMR of ethylene oligomerization products formed in the reaction catalyzed by $[Ni_3(ndc)_3(DMF)_2((CH_3)_2NH)_2]_n$ (**3**) at 1 bar ethylene pressure and 21 °C.